**Steel and Composite Structures**, *Vol. 49, No. 1 (2023) 65-79*
https://doi.org/10.12989/scs.2023.49.1.065


# Empirical evaluations for predicting the damage of FRC wall subjected to close-in explosions

Duc-Kien Thai[1a], Thai-Hoan Pham[*2], Duy-Liem Nguyen[3a], Tran Minh Tu[4a] and Phan Van Tien[5a]

[1]*Department of Civil and Environmental Engineering, Sejong University, 98 Gunja-Dong, Gwangjin-Gu, Seoul, 143-747, South Korea*
[2]*Department of Concrete Structures, National University of Civil Engineering, 55 Giai Phong, Hanoi, Vietnam*
[3]*Department of Civil Engineering and Applied Mechanics, Ho Chi Minh City University of Technology and Education, 1 Vo Van Ngan St., Thu Duc District, Ho Chi Minh City, Vietnam*
[4]*Faculty of Industrial and Civil Engineering, National University of Civil Engineering, 55 Giai Phong, Hanoi, Vietnam*
[5]*Department of Civil Engineering, Vinh University, Vinh 461010, Vietnam*

*(Received October 18, 2021, Revised September 27, 2023, Accepted October 4, 2023)*

**Abstract.** This paper presents a development of empirical evaluations, which can be used to evaluate the damage of fiber-reinforced concrete composites (FRC) wall subjected to close-in blast loads. For this development, a combined application of numerical simulation and machine learning approaches are employed. First, finite element modeling of FRC wall under blast loading is developed and verified using experimental data. Numerical analyses are then carried out to investigate the dynamic behavior of the FRC wall under blast loading. In addition, a data set of 384 samples on the damage of FRC wall due to blast loads is then produced in order to develop machine learning models. Second, three robust machine learning models of Random Forest (RF), Support Vector Machine (SVM), and Extreme Gradient Boosting (XGBoost) are employed to propose empirical evaluations for predicting the damage of FRC wall. The proposed empirical evaluations are very useful for practical evaluation and design of FRC wall subjected to blast loads.

**Keywords:** close-in explosion; empirical evaluation; fiber reinforced concrete; LS-DYNA; wall

## 1. Introduction

Wall is an important structural component, which is extensively used in civil, industrial, and military construction. Walls can withstand in-plane forces, induced by static loads, live loads, wind loads, and earthquakes. On the other hand, walls can also withstand out-of-plane loads such as impact or explosion. Therefore, this type of structure has been interesting in research for recent years, e.g., (Bai 2020, Liu 2020). In industrial buildings, such as nuclear power plants, or in military buildings, such as ammunition depots, walls are designed to withstand extreme loads such as explosive loads, ensuring safety for people and equipment inside the building. Besides, with many outstanding features such as high tensile strength and good energy dispersion, FRC structures have been commonly used for all kinds of different structures such as columns, beams (Bengar 2020, Liu 2020) and walls (Zhang 2021). FRC walls are found to have better explosive resistance than conventional RC structures (Foglar 2015). In this study, evaluation on the damage of FRC walls subjected to blast loads is concerned.

Terrorist and military attacks by bombings may destroy buildings and structures, kill and injure many people, and cause huge economic losses. The Murrah Federal Building bombing in Oklahoma City in 1995 (https://en.wikipedia.org/wiki/Oklahoma_City_bombing) and the bombardment of Yeonpyeong by the North Korea military in 2010 (https://en.wikipedia.org/wiki/Bombardment_of_Yeonpyeong) were two of the most destructive attacks in human history. These disasters demonstrate the need for a reliable design and safety evaluation of structures to resist against the blast loading. For this purpose, the development of empirical evaluations is required in order to provide the engineers with a practical tool for the design and safety evaluation of structures. While several empirical equations and evaluations for RC wall were proposed by McVay (McVay 1988), Morishita *et al*. (Morishita 2004), and Li and Hao (Li 2014), few empirical equations for FRC structures have been proposed. Thai *et al*. (Thai 2021) proposed an equation for predicting the residual strength of FRC columns subjected to blast loading employing the finite element method and a regression approach. For slab and wall, although Nam *et al*. (Nam 2017) proposed an empirical evaluation for predicting the damage level of fiber-reinforced cementitious composite wall subjected to contact explosions, it could not be used to evaluate the damage of FRC wall under explosions that do not contact the structure. Therefore, developing empirical equations for practical design and safety evaluation of FRC walls subjected to close-in blast loading is required.

Recently, Foglar and his colleagues carried out a series of close-in explosive experiments on RC and fiber-reinforced cementitious composite panels (Foglar 2013, Foglar 2015, Foglar 2017, Hajek 2017, Hajek 2019). They

*Corresponding author, Ph.D. Professor
E-mail: hoanpt@huce.edu.vn
[a]Ph.D.



ISSN: 1229-9367 (Print), 1598-6233 (Online)

(a) Field test setup

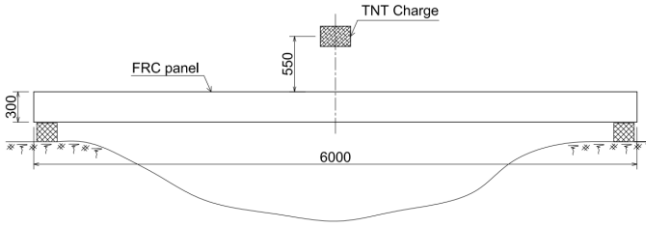


(b) Elevation view of the test

Fig. 1 Blast test setup of the FRC panels (Foglar 2017)

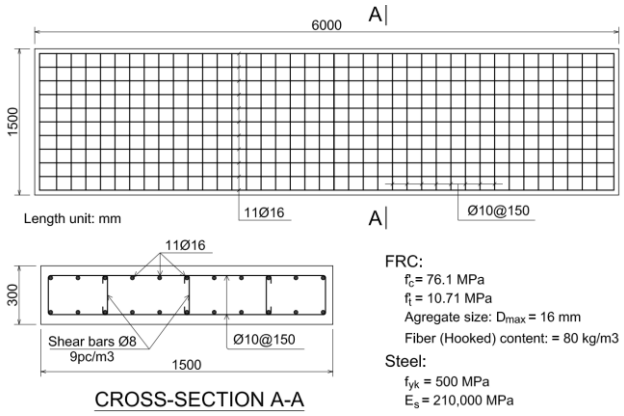


Fig. 2 Detail description of the FRC panels

performed the test using the full-scale of the panels. Many different types of concrete, fiber type and fiber content were investigated to study the damage resistance of the structures under blast loading. Moreover, some other explosive experiments on FRC panels have been also carried out by others, e.g., (Pantelides 2014, Mao 2015). In general, these tests provided a very important and realistic data for engineers and researchers. However, further studies are needed in order to provide practical tools that can be applied for practical analysis and design. Besides, numerical simulations of RC and FRC panels under blast loads have been successfully applied by some researchers (Mao 2014, Lin 2018, Hou 2019). This approach is much cheaper than the experimental method and can provide reliable results. However, since the structural behavior of FRC structures under blast loading is very complicated, the numerical simulation is often time-consuming and not easy to accurately implement by engineers. Therefore, it still requires a simpler and more accurate tool for the practical design of structures.

This study proposes a new approach which is a combination of numerical simulation and machine learning approaches, to propose the empirical evaluations on the damage of FRC wall due to the close-in explosion. For this purpose, the full-scale finite element model of FRC wall and explosion are developed. The developed modeling are then validated using the field test data of Foglar *et al*. (Foglar 2017). Based on that, parametric analysis is carried out with different parameters such as panel thickness, concrete strength, fiber type, its content, and explosive level. 384 analysis results provide a dataset for developing a technical tool for evaluating the damage level of the wall under different loading conditions. Employing some robust machine learning models, a prediction model is developed, and an empirical evaluation for practical design is provided as the important outcome of this research.

## 2. Development of FE modeling of FRC wall under blast loading

A development of FE modeling of FRC wall subjected to an explosion was carried out based on the full-scale blast test of FRC panel, conducted by Foglar *et al*. (Foglar 2017). The FRC wall with its reinforcement and boundary condition, and explosive charge with air domain are modeled using LS-DYNA. Nonlinearity material models considering strain rate effect are adopted for structural components. Multi-Material Arbitrary Lagrangian Eulerian (MM-ALE) method, the most robust simulation for explosive pressure, is employed to model the blast loading. The reliability of the developed modeling is validated by comparing its analysis results with that of the test. This section describes the development and verification of the FE modeling.

### *2.1 Full-scale blast test on FRC panel*

#### *2.1.1 Experiment description*

Foglar and his colleagues conducted a series of blast tests on the full-scale panels with different concrete mixes and reinforcement. Among those, a full-scale blast test on FRC panels, i.e., specimen No. 15 is adopted for this simulation (Foglar 2017). Fig. 1 shows the description of the field blats test. The pre-cast FRC panel was placed on two timber slats, which were fixed on the rock bed to ensure minimum settlement. The TNT charge of 25 kg was set in the middle of the panel using a steel chair, providing a standoff distance of 0.55 m from the top surface of the panel. To avoid the effect of the shock wave, which may bounce off the ground, the ground under the panel was excavated to a depth of about 2 m.

The specimen has a length of 6 m, a width of 1.5 m, and a thickness of 0.3 m. FRC having compressive strength of 76.1 MPa and tensile strength of 10.71 MPa was used for the panel. Hooked fiber having a length of 30 mm was mixed in the FRC with a ratio of 80 kg/m$^3$ (i.e., fiber content of 1%). 11 steel longitudinal bars of 16 mm in diameter were installed on both surfaces of the panel. Transverse bars being 10 mm in diameter with a spacing of 150 mm were placed transversely to form a reinforcing mesh. Shear reinforcements using the links of 8 mm in diameter were also installed with 9 pcs/m$^3$, to keep the top reinforcement mesh not deforming. All reinforcement steel

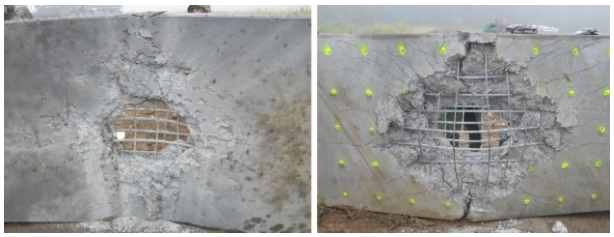

(a) Top view (b) Bottom view

Fig. 3 Damage of the panel after the blast test (Foglar 2017)

had a yielding strength of 500 Mpa and an elastic modulus of 210,000 MPa. The concrete cover was 50 mm, which is normally used in reinforced concrete structures. Fig. 2 shows the description of the design of the FRC panels.

#### *2.1.2 Test results*

The damage of the panels was observed as the main outcome of the blast test. A high-speed camera was used to record the response of the panels. Through this camera, the spalling formation on the soffit of the panels was observed. Fig. 3 shows the damage on the top and bottom of the FRC panels after the blast test. It is shown that the panel was completely perforated and collapsed. A large hole was formed at the center of the panel, and the reinforcement was deformed significantly. Some large fractures also formed on either side of the spalling hole. The measurement showed that the puncture area on the top surface was 0.16 $m^2$, and the volume of crushed concrete was 0.16 $m^3$. Meanwhile, the residual maximum deflection of the panel was about 0.5 m. This observation of damage of the FRC panels will be used for evaluating the developed FE models in the next steps.

### *2.2 Numerical modelling development*

#### *2.2.1 FE modelling development*

A full 3D models of FRC wall and TNT charge in an air domain are developed using LS-Prepost_R.4.7, as shown in Fig. 4. FRC wall is modeled using eight-nodes solid element. To obtain a reliable dynamic behavior of the structure, a fine mesh of 15 mm is used for the middle region of the wall where the local damage occurs due to the explosion, whereas the region at both sides is modeled with a coarse mesh of 30 mm, to reduce the computational cost (see Fig. 4(a)). These mesh sizes are used based on the author's experience in many similar numerical analyses and will be proven by verification with the test data, presented in the next step. Fig. 4(b) illustrates the finite element model of the reinforcement. The longitudinal rebars, transverse bars, and shear bars (links) are modeled employing the Belytschko-Schwer beam element. To model the bond-slip between concrete and rebars, LS-DYNA provides a very robust and convenient technique, that is constrained Lagrange-in-solid, in which, the concrete part and rebar part are simply defined as the master and slave parts, respectively. This technique has proved its effectiveness in simulating similar problems, e.g., (Thai 2019, Thai 2020). Two rollers are approximately modeled

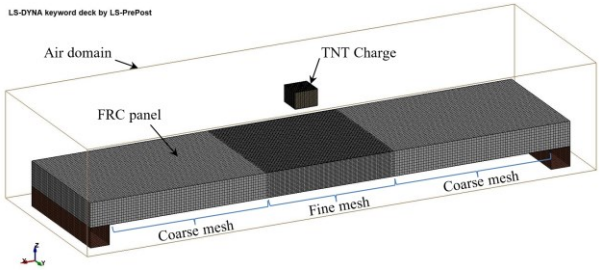


(a) Full 3D FE modelling

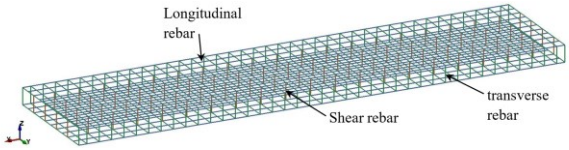


(b) Details of reinforcement modeling

Fig. 4 FE modeling of FRC wall and explosion

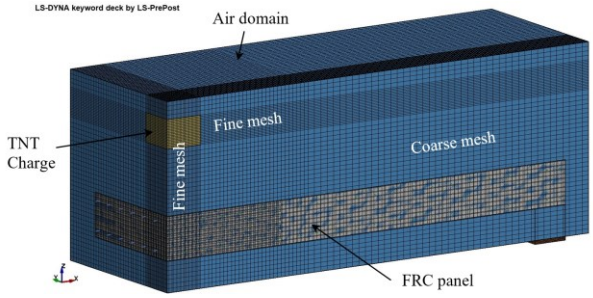


Fig. 5 Details of the meshing

as the hollow tube steel beams, using shell elements. It is noted that in the test, two timber slats were used. However, since using material model for timber may cost much more computational time, and the structural behavior of the roller itself does not have a significant influence on the response of the FRC wall under blast load, as stated in (Foglar 2017), the alternative model of the rollers using hollow tube steel beams is simpler and keeps the original response of the wall. The rollers are assumed to be fixed into the rock bed, which is consistent with the real test that the timber slats were fixed in the dug-in rock bed using steel tubes. The interaction between the rollers and the wall is modeled using the contact Surface_to_Surface in LS-DYNA.

Fig. 5 describes the correlation between the air domain and other parts of the model. With the achievements in simulating concrete structures under explosive loads in recent years, this study continues to use the blast load simulation using the Multi-Material Arbitrary Lagrangian Eulerian (MM-ALE) method. This method has been successfully used in the previous works, e.g., (Thai 2020, Thai 2021). The 1-point Arbitrary Lagrangian Eulerian (ALE) multi-material element is employed to model the air domain and the TNT charge. It is emphasized that the explosive charge must be modeled with very fine mesh, i.e., about 10 mm, as recommended in (Thai 2019). Moreover, the region near the center of the wall where the local damage occurred as shown in the test, should also be modeled with finer mesh. While, in places where the effect of the explosive pressure was trivial, coaster meshes may be

used. Therefore, in this model, the region directly related to explosives is divided with a very fine mesh, i.e., 10 mm. Regions surrounding the area where local damage is anticipated to occur, are divided with a coaster mesh of about 30 mm. While the remaining areas where the local damage is unlikely occur, are divided with a large mesh size of about 50 mm. To model the interaction between the MM-ALE domain and structural parts, the fluid-structure interaction model is employed. In this way, the explosive pressure generated by the explosive material is transmitted through the atmosphere modeled by the MM-ALE domain and transmitted to the structures.

#### *2.2.2 The used material models*

For a reliable numerical simulation, the use of the appropriate material models is extremely important. Based on the experience and know-how of the authors, in this developed FE model, different material models available in LS-DYNA (Corporation 2007) are selected, including Elastic Plastic, High Explosive Burn, Null, and Winfrith Concrete models. All these material models have been successfully used in similar works (Thai 2018, Thai 2020, Thai 2021). For the convenience of the readers, this section briefly describes these material models.

##### *a) Elastic Plastic model (MAT#003)*

The Elastic Plastic material model is the simplest model, suitable for use as typical ductile material such as construction steel. This model provides optional hardening behaviors of material, which may combine between Isotropic and Kinematic hardening by varying a parameter, called $\beta$ between 0 and 1. For $\beta = 0$, kinematic hardening is obtained, whereas, for $\beta = 1$, isotropic hardening is obtained (Corporation 2006). For the isotropic option, the center of the yield surface is fixed while its radius is a function of the plastic strain. On the contrary, for the kinematic option, the radius of the yield surface is fixed while its center translates in the direction of the plastic strain. For mild steel, kinematic hardening option is used, i.e., $\beta = 0$.

The yield condition of the Elastic Plastic material model is expressed as

$$\phi = \frac{1}{2}\xi_{ij}\xi_{ij} - \frac{\sigma_y^2}{3} = 0 \tag{1}$$

in which, $\xi_{ij} = s_{ij} - \alpha_{ij}$, where $s_{ij}$ is the stress tensor; and $\alpha_{ij}$ is the shift-stress tensor.

To consider the strain rate effect, the Elastic Plastic material model uses a well-known equation, called the Cowper-Symonds equation, which estimates the dynamic increment factor as the function of strain rate and the Cowper-Symonds constants, that depends on the material.

##### *b) High Explosive Burn model (MAT#008)*

The High Explosive Burn model is normally used for TNT explosive charges. This material model should be used along with the Jones-Wilkins-Lee (JWL) Equation of State (EoS) function (Corporation 2006). The effective pressure, $p$, in the explosive is determined by multiplying the burn fraction, $F$, and the pressure, $p_{eos}$, which is calculated by the EOS.

$$p = F \times p_{eos} \tag{2}$$

$$F = \max(F_1, F_2) \tag{3}$$

$$F_1 = \begin{cases} \dfrac{2(t-t_1)D}{3\left(\dfrac{v_e}{A_{e\max}}\right)} & \text{if } t > t_l \\ 0 & \text{if } t \le t_l \end{cases} \tag{4}$$

$$F_2 = \frac{1-V}{1-V_{CJ}} \tag{5}$$

where: $t$ is the current time; $t_l$ is the lighting time of an element; $D$ is the detonation velocity; $v_e$ is the element volume; $A_{emax}$ is the area of the largest side of an element; $V$ is the relative volume; and $V_{CJ}$ is the Chapman-Jouguet relative volume.

The JWL Equation of State function is the pressure-volume relationship on the expansion isentropic and is expressed as

$$p_{eos} = A\left(1 - \frac{\omega}{R_1 V_0}\right)e^{-R_1 V_0} + B\left(1 - \frac{\omega}{R_2 V_0}\right)e^{-R_2 V_0} + \frac{\omega E_0}{V_0} \tag{6}$$

where $p_{eos}$ is the pressure; $V_0$ is the relative volume; $E_0$ is the specific internal energy; and $A$, $B$, $R_1$, $R_2$, and $\omega$ are constants, which are calibrated using the test data.

##### *c) Null model (MAT#009)*

The air domain is modeled as an ideal gas using the combination of Null material model and the Linear Polynomial EOS. The pressure in the air domain is calculated by

$$p = C_0 + C_1\mu + C_2\mu^2 + C_3\mu^3 + (C_4 + C_5\mu + C_6\mu^2)E_0 \tag{7a}$$

where $C_0 \sim C_6$ are constants; $E_0$ is internal energy per initial volume; and $\mu = \rho/\rho_0 - 1$, here, $\rho_0$ the initial density, while $\rho$ the current density of air.

For ideal gas, $C_0 = C_1 = C_2 = C_3 = C_6 = 0$, and $C_4 = C_5 = \gamma - 1$, Eq. (7a) now becomes

$$p = (\gamma - 1)\frac{\rho}{\rho_0}E_0 \tag{7b}$$

in which, $\gamma$ is the heat ratio.

##### *d) Winfrith Concrete model (MAT#084)*

Among many material models developed for concrete, Winfrith is the most robust and effective material model, suitably used for modeling the punching behavior of structures. First, the Winfrith model considers the plasticity and optional strain rate effect, which is needed for the modeling of structures subjected to dynamic and extreme loads such as impact and blast loads. Second, it requires very few input parameters like compressive strength, tensile strength, or elastic modulus, etc. One of the advantages of

the Winfrith concrete model is capable of capturing the cracking pattern of the concrete element, which is highly useful in evaluating the damage region of the structures. Moreover, this material model considers the strain softening behavior in tension, which provides the possibility to calibrate the tensile behavior and strength of the FRC.

The Winfrith concrete was developed by Schwer (Schwer 2010) using the Ottonsen's shear failure surface model, expressed as

$$F(I_1, J_2, \cos 3\theta) = a\frac{J_2}{\left(f_c^{'}\right)^2} + \lambda\frac{\sqrt{J_2}}{f_c^{'}} + b\frac{I_1}{f_c^{'}} - 1 \quad (8)$$

here, $I_1$ is the first invariant of stress tensor; $J_2$ is the second invariant of deviatoric stress tensor; $\lambda = \lambda(\cos 3\theta)$ is the function that controls the shape of the shear failure on the $\pi$-plane; $a$ and $b$ are constants; and $f_c^{'}$ is the concrete strength in compression.

It is emphasized that there is no material model in LS-DYNA developed for FRC material. In this study, the Winfrith concrete model is used in which the tensile strength and elastic modulus of the FRC are determined as the function of fiber type and its contents. The tensile strength is calculated using the Naaman (Naaman 1972) model, whereas the elastic modulus is determined using the proposed equation of Lee *et al*. (Lee 2015), which will be presented in detail in Sub-section 3.1.

The Winfrith concrete model considers the strain rate effect optionally. The well-known strain rate effect model of CEB-FIP (CEB-FIP 1993) is employed to estimate the dynamic increment factors for tension strength, compressive strength, and elastic modulus. The biggest disadvantage of the Winfrith model is that it does not provide a model for considering damage and failure, therefore, an erosion option is needed for this purpose. Nevertheless, it should be emphasized that the erosion values are not the physical parameters, but it mainly depends on the finite element size. Therefore, sensitivity analysis is required to justify an appropriate erosion value.

### *2.3 Verification of the developed models*

For a modeling of structures subjected to blast loads, two separate validations should be made, they are (1) validation on the development of FE model of an explosion, and (2) validation on the structural behavior of the structures under blast loading. The validation on the modeling of an explosion has been made by the authors in previous research, thus, it is briefly presented in this paper for the convenience of the readers. Whereas the validation of the damage of the FRC wall under TNT charge using the test data is presented in this sub-section in more detail.

#### *2.3.1 Verification of explosive model*

For the validation of the explosive model, the explosive test conducted by Remennikov *et al*. (Remennikov 2017), and the Baker empirical equation (Baker 1973) are used. In the explosive test, Remennikov *et al*. conducted a blast testing shot of 1.0 kg equivalent TNT. The TNT charge was

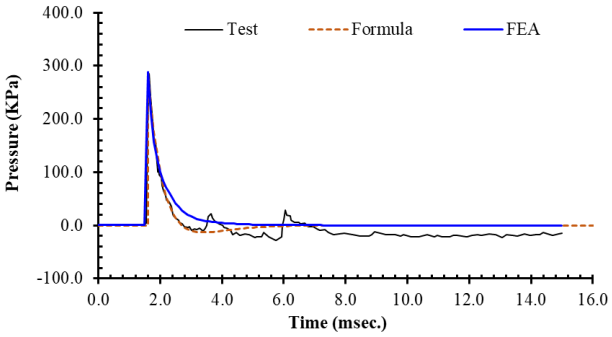


Fig. 6 Validation of pressure-time histories

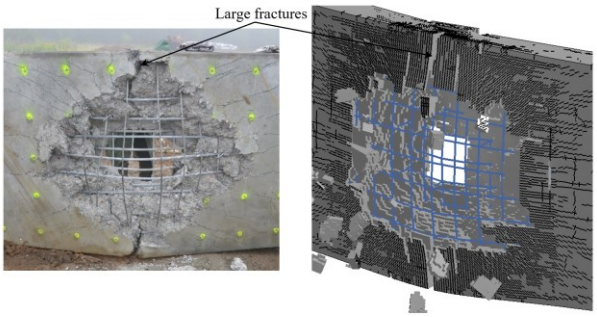


(a) Tested by Foglar *et al*. (b) FEA result in this study

Fig. 7 Comparison of damage of FRC walls

located in the mid-air. Pressure-time history was measured using the pressure gages. The pressure-time history can be estimated using the Baker equation, which is expressed as

$$P_{ex}(t) = P_{S0}\left(1 - \frac{t}{t_0}\right)e^{\frac{-\alpha t}{t_0}} \quad (9)$$

where $t_0$ and $t$ represent positive pressure duration and the current time, respectively; $P_{S0}$ is the overpressure peak (in bar); and $\alpha$ is the parameter of attenuation.

The blast test is also modeled in LS-DYNA using MM-ALE simulation as described in the previous subsection. The TNT charge is modeled using the High Explosive Burn material model incorporating the JWL EOS, whereas the air domain is modeled using the Null material model combined with the Linear Polynomial EOS. All of the input parameters for the TNT charge, free air, and EOSs are adopted from the previous paper, i.e., (Thai 2019). Fig. 6 compares the pressure-time histories obtained from the actual test of Remennikov *et al*., the Baker equation, and FE analysis. It is shown that FE analysis method can model an accurate pressure of a TNT charge. Thus, the FE model of TNT charge developed in this study using MM-ALE simulation can be reliably used in the numerical simulation of structures subjected to blast loading.

#### *2.3.2 Verification of structural model*

Although all experiments tested by Foglar *et al*. (Foglar 2017) could be used for verification, however, due to the limit of the length of the paper, only one Foglar's experiment, i.e., speciment no. 15 was used for

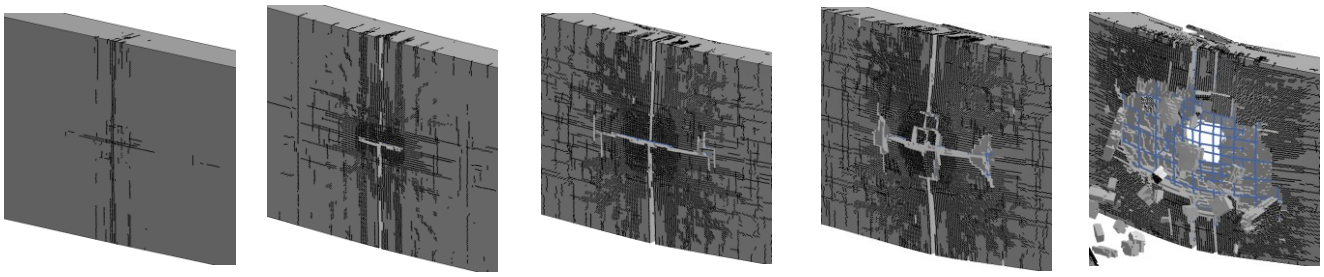

(a) No damage (b) Slight (c) Medium (d) Severe (e) Collapse

Fig. 8 Typical damage of different damage modes

Table 1 Comparison of results

| Results | Test Result | FEA Result | Difference |
|---|---|---|---|
| Residual deflection (m) | 0.5 | 0.472 | 5.60% |
| Volume of crushed concrete ($m^3$) | 0.16 | 0.17 | 6.25% |

comparision. To evaluate the accuracy of the developed model, the damage of the wall, the residual deflection, and the crushed concrete volume are compared. Fig. 7 shows the comparison of damage, while Table 1 compares the deflection and crushed volume between the test and FE analysis. It is shown that the FE analysis captures the damage to the wall accurately. A cone spalling is preached at the middle of the wall. The rebars are deformed significantly but not broken. Large fractures occur on either side of the wall edge indicating that the wall is completely failure. The comparison of residual deflection and volume of crushed concrete shown in Table 1 also indicates that the analysis results agree well with the test data. The differences in residual deflection and crushed volume are 5.60% and 6.25%, respectively. These comparisons lead to the conclusion that the numerical simulation accurately predicts the damage of the FRC walls under blast loading, thus, it can be reliably used for further analyses.

## 3. Numerical investigation on the damage of FRC wall

This section investigates the influence of different parameters on the damage of FRC wall. Parametric analyses with various parameters of wall thickness, blast level, concrete strength, and fiber content are carried out based on the validated FE model. Damage level, in terms of damage mode, is observed as the result of the analysis. Five damage modes, referred to the classification of Thai and Kim (Thai 2018), are classified as following:

• *No Damage (No)*: Some minor cracking occurs on the surface of the wall, but no fractures or spalling.

• *Slight Damage (Sl)*: Minor cracking and slight fractures occur, but the rebar is still covered by the concrete cover layer.

• *Medium Damage (Me)*: Cracking and fractures occur, concrete cover layer on the wall surface is spall, but the rebar is prevented from failure.

• *Severe Damage (Se)*: The wall is damaged very significantly, a part of the section is spall, the rebar is deformed, but the collapse mode is prevented.

• *Collapse (Co)*: The wall collapsed under the blast event.

Fig. 8 illustrates the typical damage of different damage modes of FRC wall under blast loads. These damage classifications will be used for discussions in the remainder of this paper, as well as in the development of an empirical evaluation of damage of FRC walls, which can be used in practical design.

### 3.1 Analysis parameters

Parametric studies are carried out with different parameters. Using the FRC wall described in the previous section, the thickness of the wall is varied from 240 mm to 420 mm. With this parametric study, the effect of the wall thickness on the global and local behavior of the wall is investigated and discussed. The second parameter used in this analysis is the weight of the explosive. To change the blast load level without changing the model size to avoid the increment of computational cost, the standoff distance is kept constant while the explosive weight is changed from 10 kg to 25 kg, which corresponds to the scaled distance changes from 0.028 $m/kg^{1/3}$ to 0.021 $m/kg^{1/3}$. The effect of compressive strength of the concrete matrix is investigated to see how it influences the damage of the wall. In this study, two compressive strengths of 60 MPa and 80 MPa are used, since these strengths are commonly used in civil and industrial construction. Moreover, fiber type and its content are expected to have some influence on the behavior and damage of the wall under blast loading and are therefore considered as the input parameters. Hooked and Twisted fibers, which are commonly used in construction, are selected. For each fiber type, different fiber content from 0.75% to 2.00% are varied to investigate how its influence on the explosion resistance of the wall.

As mentioned in the previous section, for the Winfrith concrete model, the tensile strength of FRC is calculated using the Naaman (Naaman 1972) model, whereas its elastic modulus is determined using the proposed equation

Table 2 Variables used for parametric analysis

| Variables | Unit | Values |
|---|---|---|
| Wall thickness | mm | 240; 300; 360; 420 |
| TNT weight | kg | 10; 13; 16; 19; 22; 25 |
| Compressive strength | MPa | 60; 80 |
| Tensile strength | MPa | 5.75; 7.18; 8.37; 9.29; 10.2; 10.42; 12.41; 12.69 |
| Elastic modulus | GPa | 25.6; 26.6; 27.4; 27.6; 28.1; 28.5; 28.9; 30.0; 30.8; 31.1; 31.6; 32.0 |

of Lee *et al*. (Lee 2015).

According to the Naaman (Naaman 1972) model, the ultimate tensile strength of FRC can be calculated as

• For strain-softening behavior

$$f_t^{'} = f_{tm}^{'}(1-V_f) + \alpha\tau V_f \frac{l_f}{d_f} \tag{10}$$

• For strain-hardening behavior

$$f_t^{'} = \lambda_{pc}\tau V_f \frac{l_f}{d_f} \tag{11}$$

where $f'_{tm}$ is the tensile strength of the matrix; $V_f$ is the fiber content; $l_f$ and $d_f$ are the fiber length and diameter, representative; $\tau$, $\alpha$, and $\lambda_{pc}$ are the equivalent bond strength, average stress factor, and average pullout length factor, respectively, determined using the test data.

The elastic modulus of FRC can be estimated as fiber type and its content, using Lee *et al*.'s (Lee 2015) equation, expressed as

$$E_c = \left(-367V_f \frac{l_f}{d_f} + 5520\right) f_{cm}^{0.41} \tag{12}$$

where $f_{cm}$ is the ultimate compressive strength of the matrix.

Table 2 summarizes the variables and their respective values used in this parametric analysis.

In Table 2, the use of two different fiber types with four content levels each result in eight types of tensile strength. Meanwhile, combining two concrete strengths with two types of fiber reinforcement with four content levels, after eliminating two coincide pairs, created twelve types of moduli.

The combination of these input variable induces 384 different analyses, which provides an abundant dataset for parametric investigation and developing the evaluation models using the Machine Learning approach, which is presented in the next part of this paper.

### *3.2 Effect of different parameters*

#### *3.2.1 Effect of wall thickness*

To investigate the effect of the thickness on the damage resistance of the wall, all other parameters are kept as constant, while the thickness is increased from 240 mm to 420.

The thickness of the wall has a significant effect on its damage, as shown in Fig. 9. As expected, as the thickness increases, the local damage decreases significantly. With the thickness of 240 mm, the wall is totally damage with a preached hole at the middle and a large fracture occurs crossing section of the wall. Rebars are deformed significantly. Moreover, small cracks occur around the preached hole. In case of the thickness equals to 300 mm, the large fracture occurs crossing the section of the wall, but the wall is prevented from fully breaching. Cracks around the middle zone appear to be wider and parallel to the large fracture at the middle of the wall. Rebars are still deformed significantly, and a severe damage occurs in this case. When the thickness increases to 360 mm, the large fracture still appears at the middle of the wall, although less spalling occurs. The cracks around the mid-wall area continue to expand parallel to the large fracture. Deformation of the rebar is reduced significantly, but the wall is still damaged quite severely. In case the thickness is equal to 420 mm, the concrete cover on the back face of the wall is spalled, but no significant damage occurs. The fracture at the mid-crossing section is not very large, while there are some small fractures occurring around the middle area. It is observed that increasing the thickness can reduce the damage level of the wall, but the cracks and fractures are seemingly dispersed over a wider area.

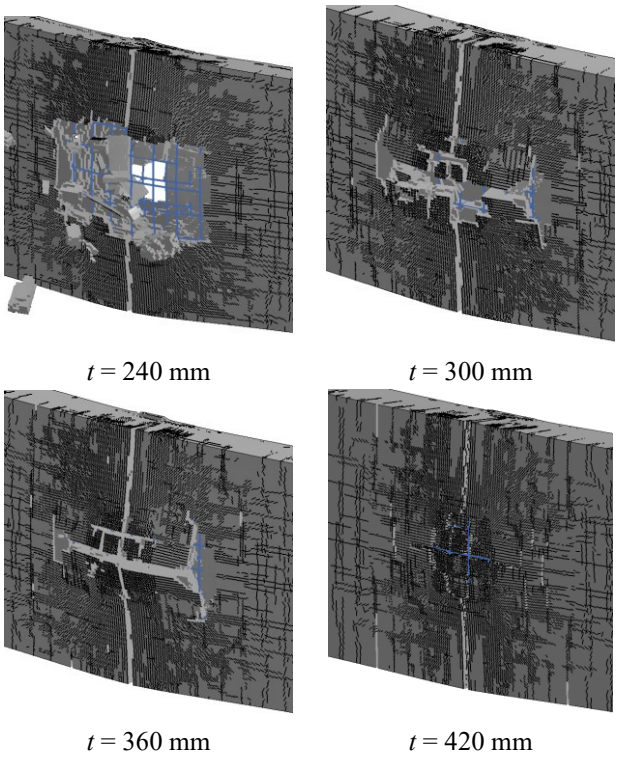


Fig. 9 Damage of walls with different thickness

#### *3.2.2 Effect of loading level*

The loading level is increased by increasing the weight of the explosive from 10 kg to 25 kg, while keeping the standoff distance as constant. By doing this, the size of the model does not change significantly, meaning that the computational time is not significantly increased.

Fig. 10 compares the damage of the wall under different blast loading levels. Of course, the blast loading level also

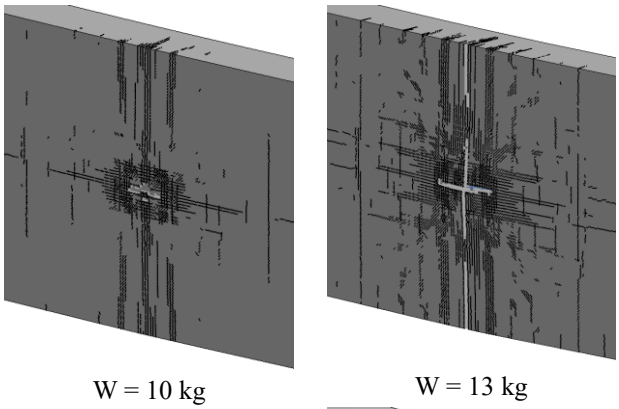


Fig. 10 Damage of wall with different load levels

has a great influence on the damage of the wall. More specifically, in case the charge weight equals 10 kg, small scabbing occurs at the center of the wall and some cracking patterns appear horizontally and in the middle of the wall. The wall is slightly damaged in this case. When the charge weight equals 13 kg, a fracture begins to form across the wall. A longitudinal fracture also appears at the center of the wall, with many small cracks appearing. At the same time, the overall and local deflection are both increased. When the charge weight is equal to 19 kg, both horizontal and longitudinal fractures are larger and expose the reinforcement and a significant cracking pattern appears in the middle area of the wall. A large deflection occurs, and local failure begins to form. When the explosive charge increases to 25 kg, severe damage occurs locally. A large scabbing hole appears exposing the reinforcement. A large fracture also appears across the wall making the wall about to break. Small cracks are also more widespread.

In general, increasing the blast loading level makes local damage, global deformation, and the deformation of the rebars increase significantly, at the same time, the fracture and cracking pattern also increase until the wall is completely collapsed.

### *3.2.3 Effect of concrete strength*

In this study, we focus on the FRC with normal strength concrete. Therefore, the concrete strengths from 60 MPa to 80 MPa are considered in this analysis. Based on the author's experience, although the compressive strength of concrete has some effect to the damage of the wall, this parameter is not a sensitive one, therefore only two values

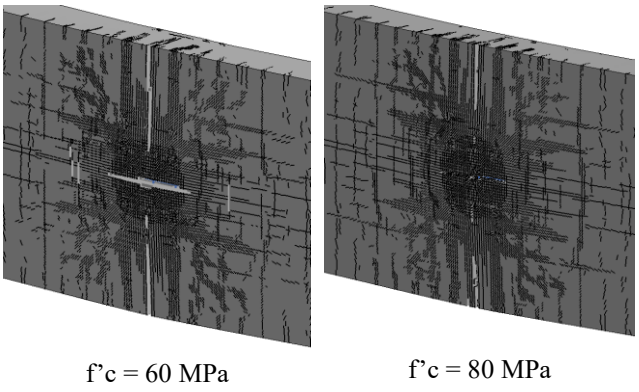


Fig. 11 Damage of wall with different concrete strengths

of strength are selected, i.e., 60 MPa and 80 MPa.

Unlike the parameters of wall thickness and loading level, the concrete strength, although having some effect on the damage of the FRC wall, is not very significant, as shown in Fig. 11. Analysis results show that the wall using concrete compressive strength of 60 MPa has a larger fracture than compared to the one using strength of 80 MPa. While the wall with 60 MPa in compressive strength appear to have more fractures around the center area, the wall with 80 MPa in compressive strength only forms with two main fractures, i.e., horizontal and longitudinal fractures. In the first wall, the reinforcement was exposed more significantly than the second wall, indicating that the first wall is deformed more significantly. It can be concluded that, although the change in compressive strength of concrete does not change the damage modes (i.e., in both cases, the slight damage mode occurs), there is a change in the failure level of the wall.

### *3.2.4 Effect of fiber content*

The fiber type and its content alter the ultimate tensile strength and are therefore expected to increase the damage resistance of the FRC wall. In this simulation, the fiber type and its content are considered as the ultimate tensile strength, calculated using Naaman equations (Naaman 1972). It is clear that Twisted fiber has a greater effect on the damage resistance of the wall than Hooked fibers. Thus, in this analysis only the effect of the maximum tensile strength on the damage of the wall is investigated, using Hooked fiber, changing the content from 0.75% to 2.00%, the content range is commonly used in construction.

Fiber reinforcement is generally expected to have a significant effect on minimizing the failure of the wall under explosive loads. However, analysis results in this study revealed that increasing the fiber content does not significantly increase the explosion resistance as shown in Fig. 12. The difference found here seems to be just the distribution of cracks on the concrete wall. When the fiber content is low, i.e., 0.75%, the major fracture appears concentrated at the midpoint across the wall, while in case of a higher fiber content, e.g., 2.00%, the fractures seem to be distributed to either side of the wall, at the same time, the number of small cracks is reduced. The fiber content has a slight effect on reducing the deflection of the wall as shown in Fig. 13. Therefore, the reduction in deflection of the wall

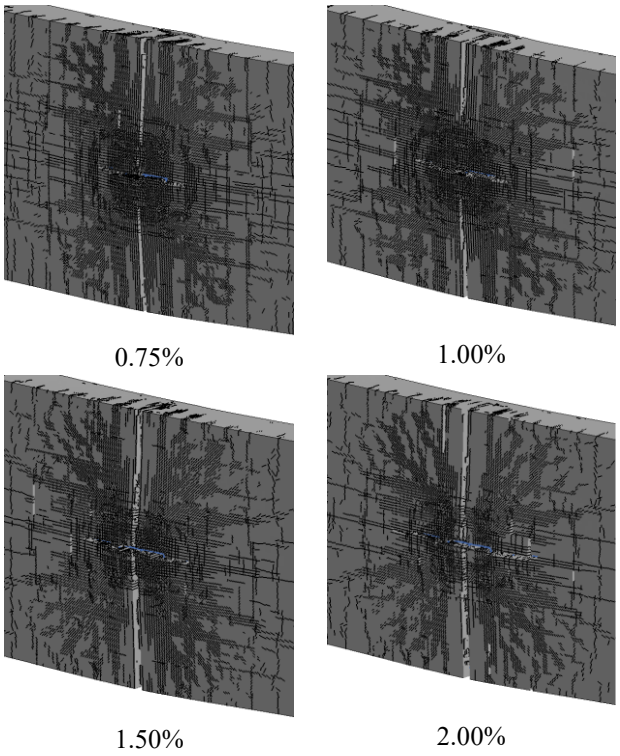


Fig. 12 Damage of wall with different fiber contents

is negligible.

This observation should have been verified by experimental data. Unfortunately, no experimental data were available regarding the effect of fiber content (with the usual ranges used in this analysis) on the blast resistance of the wall. While experimental results by Hajek *et al*. (Hajek 2017) revealed that low-performance steel fiber has no significant effect on blast resistance of the wall, the test data conducted by Yao *et al*. (Yao 2020) showed that, FRC wall resulted in the best resistance compared to hybrid fiber wall (which are the combinations between steel, polypropylene, and polyvinyl alcohol fibers). In the tests of Foglar *et al*. (Foglar 2015), where a different fiber content of 0.5% to 1.0% was used, all the wall were destroyed, so it was not possible to evaluate the influence of the fiber content on the explosion resistance of the wall. Theoretically, the fiber reinforcement increases the tensile strength of the material, thereby also increasing the flexural resistance of the wall, that is, reducing deflection, as observed in this analysis. For components under high-speed loads such as impact and blast loads, reducing deflection (i.e., increasing the stiffness of the wall) may result in a severer local damage of the wall. Only when the thickness of the wall is great enough so that increasing the stiffness does not significantly reduce the deformation of the wall, then the tensile strength of the material may reduce the damage to the wall.

Analysis results investigated in this section show that each parameter has some effect on the damage of the FRC wall. Although the concrete strength and fiber content, separately, did not seem to have much effect on the blast resistance of the structure, the analysis also showed a collaborative effect. For example, increasing the thickness and content of the fiber at the same time may increase the

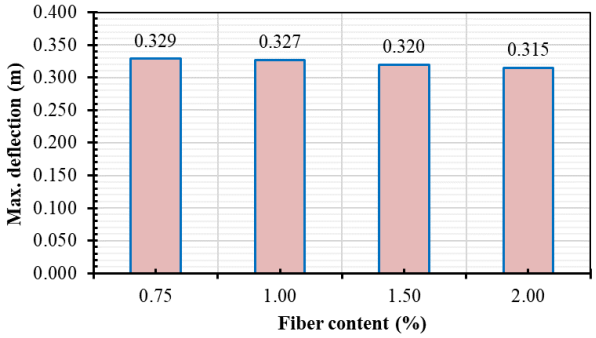


Fig. 13 Max. deflection vs fiber content

explosion resistance of the wall, while increasing the fiber content without increasing the wall thickness may reduce its explosion resistance. Therefore, it is necessary to consider the effect of all parameters in a reciprocal way. Thus, the next section will present the development of the empirical evaluations for the FRC wall considering all the parameter's effects.

## 4. Development of empirical evaluation

In this section, an empirical evaluation model is developed to predict the damage of FRC wall under blast loading using machine learning (ML) algorithms. A dataset obtained from the parametric study using the developed finite element model is used to train the ML algorithms. Since there are five different damage modes of the FRC wall, it requires using the multiclass classification algorithms to learn the dataset. Three well-known supervised ML classifiers are selected to establish the damage classification model including the Random Forest (RF), Support Vector Machine (SVM), and Extreme gradient boosting (XGBoost). The final ML model is expected to accurately classify the damage mode of an FRC wall among the five typical damage modes. A graphical user interface (GUI) application is developed for the practical use of the developed ML model. Finally, a simplified evaluation graph is established to rapidly predict the damage of the FRC wall under the blast loading.

### *4.1 Machine learning models*

#### *4.1.1 Random Forest (RF)*

Random forest (RF) (Ho 1995) is an ensemble-based learning algorithm using the decision tree classifier (Breiman 1984) as a base learner. Each decision tree conducts a complete classification of damages based on the given features. Its result presents a possible solution for the classification problem. RF is a statistical learning algorithm that extracts several samples from the original dataset using the bootstrap resampling process, the decision tree is applied for each bootstrap set, and then the results of multiple decision trees are combined for the final classification results. By this mechanism, the RF classifier can obtain a more accurate classification and reduce the overfitting issue of the single decision tree. The RF

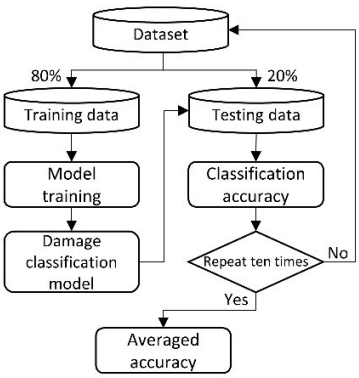


Fig. 14 Blast damage classification procedure of FRC wall

classifier is selected because it is a strong algorithm that exhibits satisfactory outcomes in the multiclass classification scenario.

#### 4.1.2 Extreme Gradient Boosting (XGBoost)

Extreme Gradient Boosting (XGBoost) (Chen 2016) is an advanced supervised algorithm which is widely used for multiclass classification problems because of its high efficiency and flexibility. XGBoost is developed based on the Gradient Boosting framework. The difference is that it is added a regularization term to the loss function which contributes to smoothening the final learned weight to avoid the overfitting problem. The XGBoost algorithm is a robust classifier for structured or tabular data which employs a multi-threaded approach in which the CPU core of the computer is fully used, resulting in increased learning speed and performance. Thus, it has been widely used for many practical engineering problems and provided satisfactory results (Thai 2019, Dong 2020). In addition, XGBoost can extract the importance of each feature in generating the classification which reveals the most important parameters in predicting the damages of FRC wall under the blast loading.

#### 4.1.3 Support Vector Machine (SVM)

Support vector machine (SVM) is a non-probability classification algorithm based on the statistical learning theory (Boser 1992). SVM is a strong algorithm that performs well in a high-dimensional feature space. It maps the original samples to points in a higher dimension space using various kernel functions to maximize the margin between the two categories. The margin is determined by two parallel hyperplanes which separate the two classes. However, when the data points are not linearly separated and overlapped, the low-generalization discriminant hyperplanes can be obtained, which encounters the overfitting issue. To deal with this problem, the soft margin formulation is applied, in which some misclassifications can be allowed in the overlapped area between two classes. This helps to reduce the overfitting effect and produce satisfactory classification performance. For a multiclass classification problem, the one vs all strategy is applied, in which the optimal discriminant hyperplanes are found by separating one selected class from other classes by turn. This means multiple binary classification subproblems are carried out to solve a single multiclass problem. Since SVM can well classify data with complicated distributions, it has been widely used in many engineering problems (Huang 2019, Ling 2019, Doan 2021).

Table 3 Classification accuracy of each damage mode

| Classifiers | Damage modes* | | | | | |
|---|---|---|---|---|---|---|
| | No. | Sl. | Me. | Se. | Co. | Average ± STD |
| RF | 0.882 | 0.895 | 0.233 | 0.982 | 0.945 | 0.787 ± 0.312 |
| XGBoost | 0.882 | 0.916 | 0.533 | 0.982 | 0.926 | 0.848 ± 0.179 |
| SVM | 0.927 | 0.926 | 0.733 | 0.912 | 0.919 | 0.884 ± **0.084** |

* No.: No damage; Sl.: Slight; Me.: Medium; Se.: Severe; Co.: Collapse

### 4.2 Dataset description

The dataset is collected from the parametric study of the FRC wall under the blast loading using the developed finite element model. It contains 384 samples which are divided into five classes having 15, 133, 97, 85, and 54 samples which correspond to five damage modes: *No damage* (No), *Slight* (Sl), *Medium* (Me), *Severe* (Se), and *Collapse* (Co). These damage modes serve as the targeted labels $y$ in the classification. Five features represented for the input parameters are considered including $x_1$ and $x_2$ are the scaled thickness *t/W^(1/3)* and scaled distance *R/W^(1/3)*, respectively, which are calculated from the wall thickness $t$, the TNT charge weight $W$, and the distance from the charge to the FRC specimens $R$; $x_3$ is the compressive strength of concrete $f_c^{'}$; $x_4$ is the Elastic modulus of concrete $E_c$; $x_5$ is the tensile strength of concrete $f_t^{'}$.

Since the features have different scales, thus, before training they are normalized into the common range of [0, 1] to accelerate the training and obtain a better performance. In this study, the features are normalized by using the min-max normalization method presented as follows

$$\overline{x}_i = \frac{x_i - x_{\min}}{x_{\max} - x_{\min}} \tag{13}$$

where $\overline{x}_i$ is the normalized value of the corresponding original value $x_i$; $x_{\max}$ and $x_{\min}$ stand for the maximum and minimum value of the current feature, respectively.

### 4.3 Classification procedure

The three ML algorithms are trained with 80% of the dataset and tested with the remaining 20%. Since the number of samples in each class is imbalanced, the dataset is split using the stratification method, in which the percentage of samples in each class is preserved in both the training and testing set. To avoid bias training due to the stochastic characteristic of ML models, the training and testing procedure is repeated ten times and then the average

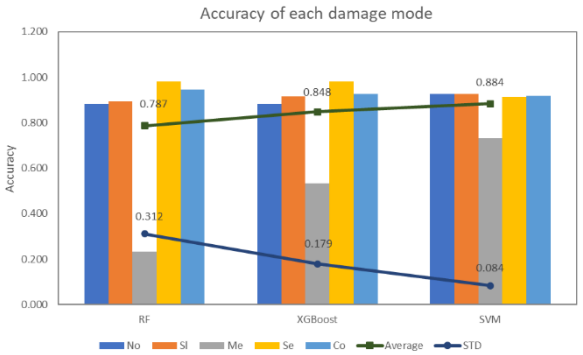


Fig. 15 Classification accuracy obtained by the three classifiers

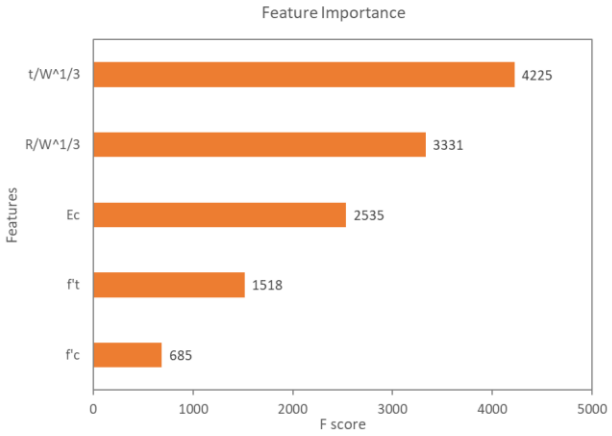


Fig. 16 Effect of each feature on the blast damage prediction obtained by the XGBoost classifier

result is outputted as the final performance. The hyperparameters of the used classifiers are selected according to their performances in the testing sets. So that the hyperparameters yielding the highest average classification accuracy will be used to establish the final model. The procedure of training and testing the blast damage classification model is illustrated in Fig. 14.

### *4.4 Classification performance*

In this section, the performances of the three classifiers including RF, XGBoost, and SVM are reported. Classification accuracy of each class, the average accuracy, and their corresponding standard deviation (STD) value are used as the evaluation metrics which are shown in Table 3 and Fig. 15. The higher accuracy presents a better prediction of the damage modes. In addition, the lower STD indicates the more balanced classification capacity of the model in each class.

As can be seen from Table 3 and Fig. 15, the SVM classifier achieves the best performance with the highest accuracy of 88.4% and the lowest STD of 8.4%. It is followed by the XGBoost classifier with a classification accuracy of 84.8% and an STD of 17.9%. The RF classifier obtained the lowest performance among the three classifiers. It can be seen that the accuracy of the *No damage*, *Slight*, *Severe*, and *Collapse* damage modes is generally high in all RF, XGBoost, and SVM classifiers in which the lowest accuracy is 88.2% and the highest is 98.2%. However, the accuracy of the *Medium* damage class is quite low, especially when using the RF classifier (i.e., 23.3%). This is because the tree-based classifiers such as RF and XGBoost use the only single feature at one tree node to classify the samples, but the samples of the *Medium* damage class are not clearly separated from the others. This leads to a higher chance of misclassification. In this Medium damage class, the SVM classifier yields the highest accuracy of 73.3% which results in its lowest STD. From the implementation results, the SVM is selected as the final classification model used to predict the blast damages of the FRC wall.

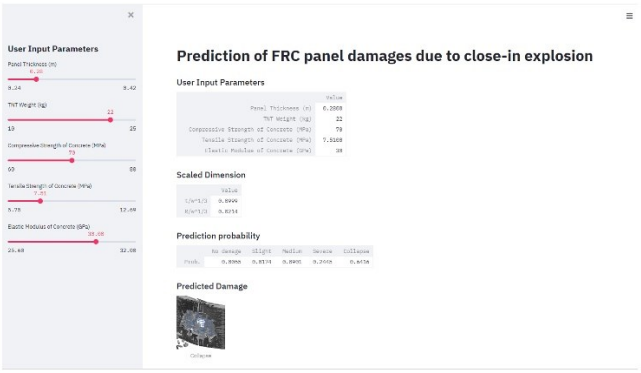


Fig. 17 A GUI application to predict the damages of FRC wall under blast loading

In order to easily estimate the importance of each parameter contributing to the damage of FRC wall, the XGBoost classifier is used since it can extract the feature that contributes the most to the classification. The feature importance is presented in Fig. 16, in which F-score is the feature weight representing the number of used times for the split in decision trees of each feature. As can be seen, the scaled thickness *t/W^(1/3)* and scaled distance *R/W^(1/3)* are the most important parameters in evaluating the damage of the wall under the blast loading. That is why only these two variables were used in the well-known empirical evaluation of McVay (McVay 1988). In addition, Fig. 16 shows that other parameters i.e., the compressive strength $f_c^{'}$ and tensile strength of the FRC concrete $f_t^{'}$, and the elastic modulus of the FRC concrete $E_c$ also affect the damage evaluation of the FRC wall. Therefore, by considering all of these parameters in evaluation, we can achieve a higher damage prediction accuracy.

For practical use of the classification model, a GUI application is developed based on the trained SVM model. The application is built using the Streamlit-an app framework that allows data scientists and ML engineers to quickly deploy an easy-to-use ML application (Streamlit Inc.). It allows users to input the five common input parameters including wall thickness, TNT charge weight, compressive strength, tensile strength, and Elastic modulus of concrete, and then output the possible damage of the given FRC wall. The application allows designers and engineers to rapidly assess the damage of an FRC wall in

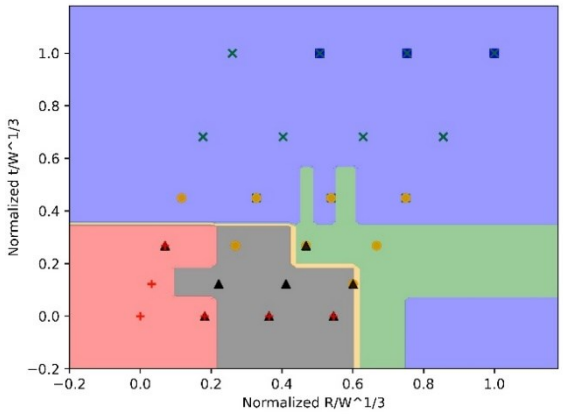


(a) Random Forest

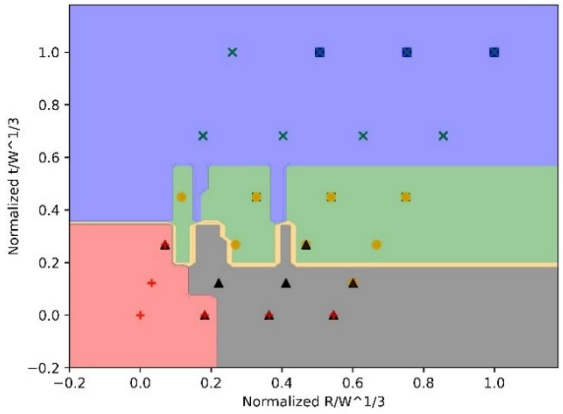


(b) XBGboost

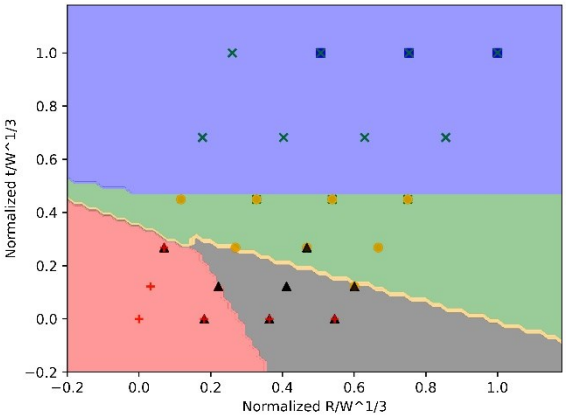


(c) SVM with linear kernel

Fig. 18 Decision boundary obtained from the three classifiers

order to provide quick decisions in designing or evaluating the structure under blast loading. The application is demonstrated in Fig. 17.

### *4.5 Empirical evaluation development*

The empirical evaluation graph proposed by McVay (McVay 1988) has been widely used to predict the damages RC wall under the blast loading. However, the evaluation graph for FRC wall has never been introduced, thus this study aims to develop an empirical evaluation graph for the quick prediction of FRC wall damages under blast loading.

As can be seen from the results of the feature importance, the scaled thickness *t/W^(1/3)* and the scaled distance *R/W^(1/3)* are the most contributing parameters to predict the blast damages of FRC wall. Thus, they can be used to create a simplified empirical evaluation graph. In this case, the dataset presented in the Appendix is used with only two variables $x_1$ and $x_2$ corresponding to *t/W^(1/3)* and *R/W^(1/3)*. The RF, XGBoost, and SVM classifier are utilized to learn the given dataset in order to provide the decision boundaries separating the damages. To obtain a quick and satisfactory performance result, the normalized features using the min-max normalization method are used. The decision boundary results obtained from the three classifiers are presented in Fig. 18, in which the SVM with the linear kernel is used for simplicity.

As can be seen from Fig. 18, the decision boundary obtained from the SVM model is appropriate for practical use. Moreover, the SVM model was found to have the best performance in predicting the blast damage of FRC wall as presented in the previous section. Therefore, the discriminant boundaries obtained from the SVM model using the linear kernel are used to develop the empirical evaluation graph.

At first, the discriminant equations are extracted by using the learning weights or coefficients achieved from the SVM model. Since the features are normalized before training the model, the final discriminant equations are built using the denormalized features. The denormalization of each feature is conducted based on the minimum and maximum values of each feature.

The decision boundaries achieved from the SVM model can be expressed as follows

$$y = w_0 + w_1 x_1 + w_2 x_2 + \ldots + w_n x_n \tag{14}$$

in which, $w_0$ is the intercept value; while $w_i$ is the $i$th learning coefficient corresponding to the feature $x_i$ among $n$ features.

In this study, the $x_1$ represents *t/W^1/3*, while $x_2$ stands for *R/W^1/3*. From the learning coefficient $w_0, w_1, w_2$ obtained from the SVM model, we have the following equations

$$y = w_0 + w_1 \bar{x}_1 + w_2 \bar{x}_2 \tag{15}$$

where $\bar{x}_1$ and $\bar{x}_2$ are the normalized features. Eq. (15) can be simplified as

$$\bar{x}_1 = -\frac{w_0}{w_1} - \frac{w_2}{w_1}\bar{x}_2 \tag{16}$$

$$\text{or} \quad \bar{x}_1 = a\bar{x}_2 + b \tag{17}$$

where $a = -\frac{w_2}{w_1}$ and $b = -\frac{w_0}{w_1}$.

Since the features were normalized by the min-max normalization with the range of [0, 1], the denormalized

discriminant equation can be expressed as follows

$$\frac{x_1 - x_{1\min}}{x_{1\max} - x_{1\min}} = a\frac{x_2 - x_{2\min}}{x_{2\max} - x_{2\min}} + b \tag{18}$$

$$x_1 = a\frac{S_1}{S_2}x_2 - ax_{2\min}\frac{S_1}{S_2} + bS_1 + x_{1\min} \tag{19}$$

where $S_1 = x_{1\max} - x_{1\min}$ and $S_2 = x_{2\max} - x_{2\min}$. For simplicity, Eq. (19) can be written as

$$y = Ax + B \tag{20}$$

with $A = a\frac{S_1}{S_2}$ and $B = -ax_{2\min}\frac{S_1}{S_2} + bS_1 + x_{1\min}$.

By using the above expressions, the SVM discriminant boundaries shown in Fig. 18(c) are appropriately selected and simplified for practical use. The final evaluation graph for the blast damages of FRC wall is presented as in Fig. 19.

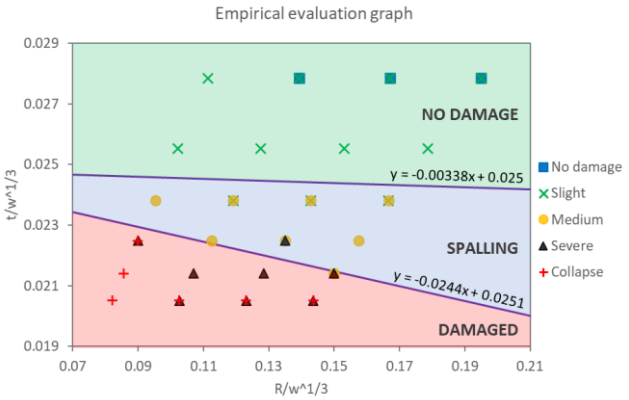


Fig. 19 Empirical damage evaluation of FRC wall subjected to the blast loading

## 5. Conclusions

The damage caused by terrorist and military attacks by bombings demonstrate the need for a reliable design and safety evaluation of structures to resist against the blast loading. For this purpose, this study proposed a novel empirical evaluation for evaluating the damage of FRC wall subjected to blast load, which is developed combining the numerical simulation and machine learning approaches. A reliable finite element modeling of FRC wall under blast loading is developed and verified using the experimental data. A parametric study is then carried out to investigate the effect of different parameters on the damage of the wall, and to produce a data set on the damage level of FRC wall. Three robust machine learning models, the Random Forest (RF), Support Vector Machine (SVM), and Extreme gradient boosting (XGBoost) are employed for developed the empirical evaluations. The following conclusions are made.

• The wall thickness and blast loading level show a significant effect on the damage level of FRC wall. Increasing the thickness of the wall can reduce the damage level of the wall, but the cracks and fractures are seemingly dispersed over a wider area. Increasing the blast loading level makes the local damage, global deformation, and the deformation of the rebars increasing significantly, at the same time, the fracture and cracking pattern also increase until the wall is completely collapsed.

• Compared to the wall thickness, concrete strength and fiber play a lower role in improving the damage resistance of the wall. While the compressive strength of concrete has a slight effect on the resistance, tensile strength combining with wall thickness may improve the resistance capacity of the walls. When the thickness of the wall is great enough, increasing the tensile strength may reduce the local damage of the walls.

• Analysis results also showed that the parameters have a collaborative effect. For example, increasing the thickness and content of the fiber at the same time may increase the explosion resistance of the wall, while increasing the fiber content without increasing the wall thickness may reduce its explosion resistance. Therefore, it is necessary to consider the effect of all parameters in a reciprocal way.

•The SVM classifier achieves the best performance with the highest accuracy of 88.4% and the lowest STD of 8.4%. It is followed by the XGBoost classifier with a classification accuracy of 84.8% and an STD of 17.9%. From the implementation results, the SVM is selected as the final classification model used to predict the blast damages of the FRC wall.

This study provides two practical tools for analysis and design of FRC walls subjected to blast load: a GUI application allows engineers to rapidly assess the damage of an FRC wall, and an empirical evaluation can be used for approximate evaluation of the damage level of the walls.

## Acknowledgments

This research is funded by Hanoi University of Civil Engineering (HUCE-Vietnam) under grant number 28-2022/KHXD-TĐ.

## References

Bai, J., Zhang, J., Du, K. and Jin, S. (2020), "A simplified seismic design method for low-rise dual frame-steel plate shear wall structures", *Steel Compos. Struct.*, **37**(4), 447-462 http://dx.doi.org/10.12989/scs.2020.37.4.447.

Baker, W.E. (1973), Explosions in Air, University of Texas Press, Austin, TX.

Bengar, H.A., Kiadehi, M.A., Shayanfar, J. and Nazari, M. (2020), "Effective flexural rigidities for RC beams and columns with steel fiber", *Steel Compos. Struct.*, **34**(3), 453-465. http://dx.doi.org/10.12989/scs.2020.34.3.453.

Boser, B.E., Guyon, I.M. and Vapnik, V.N. (1992), "A training algorithm for optimal margin classifiers", *Proc. Fifth Annu. Work. Comput. Learn. Theory*.

Breiman, L., Friedman, J., Stone, C.J. and Olshen, R.A. (1984), *Classification and Regression Trees*, Chapman and Hall/ CRC press.

CEB-FIP (1993), *Model Code 1990: Design Code*.

Chen, T. and Guestrin, C. (2016), "XGBoost: A scalable tree boosting System", CoRR. abs/1603.0.

Corporation, L.S.T. (2006), LS-DYNA Theory Manual. California.

Corporation, L.S.T. (2007), LS-DYNA Keyword User's Manual, Version 971. California.

Doan, Q.H., Le,T. and Thai, D.K. (2021), "Optimization strategies of neural networks for impact damage classification of RC panels in a small dataset", *Appl. Soft Comput.* **102**. https://doi.org/10.1016/j.asoc.2021.107100.

Dong, W., Huang, Y., Lehane, B. and Ma, G. (2020), "XGBoost algorithm-based prediction of concrete electrical resistivity for structural health monitoring", *Autom. Constr.,* **114**. https://doi.org/10.1016/j.autcon.2020.103155.

Foglar, M. and Kovar, M. (2013), "Conclusions from experimental testing of blast resistance of FRC and RC bridge decks", *Int. J. Impact. Eng.,* **59**, 18-28. https://doi.org/10.1016/j.ijimpeng.2013.03.008.

Foglar, M., Hajek, R., Fladr, J., Pachman, J. and Stoller, J. (2017), "Full-scale experimental testing of the blast resistance of HPFRC and UHPFRC bridge decks", *Construct. Build. Mater.,* **145**, 588-601. https://doi.org/10.1016/j.conbuildmat.2017.04.054.

Foglar, M., Hajek, R., Kovar, M. and Stoller, J. (2015). "Blast performance of RC panels with waste steel fibers", *Construct. Build. Mater.,* **94**, 536-546. https://doi.org/10.1016/j.conbuildmat.2015.07.082.

Hajek, R., Fladr, J., Pachman, J., Stoller, J. and Foglar, M. (2019), "An experimental evaluation of the blast resistance of heterogeneous concrete-based composite bridge decks", *Eng. Struct.,* **179**, 204-210. https://doi.org/10.1016/j.engstruct.2018.10.070.

Hajek, R., Foglar, M. and Kohoutkova, A. (2017), "Recent development in blast performance of fiber-reinforced concrete. IOP Conf. Series: Materials Science and Engineering", IOP Publishing. **246**.

Ho, T.K. (1995), "Random decision forests", *Proc. 3rd Int. Conf. Doc. Anal. Recognit*., IEEE.

Hou, X., Liu, K., Cao, S. and Rong, Q. (2019). "Factors governing dynamic response of steel-foam ceramic protected RC slabs under blast loads", *Steel Compos. Struct.,* **33**(3), 333-346. http://dx.doi.org/10.12989/scs.2019.33.3.333.

Huang, Y. and Zhao, L. (2019), "Review on landslide susceptibility mapping using support vector machines", *Catena.* **165**, 520-529. https://doi.org/10.1016/j.catena.2018.03.003.

Lee, S.C., Oh, J.H. and Cho, J.Y. (2015), "Compressive behavior of fiber-reinforced concrete with end-hooked steel fiber", *Materials,* **8**, 1442-1458. https://doi.org/10.3390/ma8041442.

Li, J. and Hao, H. (2014), "Numerical study of concrete spall damage to blast loads", *Int. J. Impact Eng.,* **68**, 41-55. https://doi.org/10.1016/j.ijimpeng.2014.02.001.

Lin, X. (2018), "Numerical simulation of blast responses of ultra-high performance fiber reinforced concrete panels with strain-rate effect", *Construct. Build. Mater.,* **176**, 371-382. https://doi.org/10.1016/j.conbuildmat.2018.05.066.

Ling, H., Qian, C., Kang, W., Liang, C. and Chen, H. (2019), "Combination of Support Vector Machine and K-Fold cross validation to predict compressive strength of concrete in marine environment", *Construct. Build. Mater.,* **206**, 355-363. https://doi.org/10.1016/j.conbuildmat.2019.02.071.

Liu, C., Wu, X., Wakil, K., Jermsittiparsert, K., Ho, S.L., Alabduljabbar, H., Alaskar, A., Alrshoudi, F., Alyousef, R. and Mohamed, A.M. (2020), "Computational estimation of the earthquake response for fibre reinforced concrete rectangular column", *Steel Compos. Struct.,* **34**(5), 743-767. http://dx.doi.org/10.12989/scs.2020.34.5.743.

Liu, J. L., Xu, L.H. and Li, Z.X. (2020), "Experimental study on component performance in steel plate shear wall with self-centering braces", *Steel Compos. Struct.,* **37**(3), 341-351. http://dx.doi.org/10.12989/scs.2020.37.3.341.

Mao, L., Barnett, S., Begg, D., Schleyer, G. and Wight, G. (2014), "Numerical simulation of ultra high performance fibre reinforced concrete panel subjected to blast loading", *Int. J. Impact. Eng.* **64**, 91-100. https://doi.org/10.1016/j.ijimpeng.2013.10.003.

Mao, L., Barnett, S.J., Tyas, A., Warren, J., Schleyer, G.K. and Zaini, S.S. (2015), "Response of small scale ultra high performance fibre reinforced concrete slabs to blast loading", *Construct. Build. Mater.,* **93**, 822-830. https://doi.org/10.1016/j.conbuildmat.2015.05.085.

McVay, M.K. (1988), *Spall damage of concrete structures - Technical Report SL-88-22*, Structures Laboratory, Department of the Army.

Morishita, M., Tanaka, H., Ando, T. and Hagiya, H. (2004), "Effects of concrete strength and reinforcing clear distance on the damage of reinforced concrete slabs subjected to contact detonations", *Concrete Res. Technol.,* **15**(2), 89-98. https://doi.org/10.3151/crt1990.15.2_89.

Naaman, A.E. (1972), A Statistical Theory of Strength for Fiber Reinforced Concrete, Ph.D Thesis, Massachusetts Institute of Technology.

Nam, J., Kim, H. and Kim, G. (2017), "Experimental investigation on the blast resistance of fiber-reinforced cementitious composite panels subjected to contact explosions", *Int. J. Concrete Struct. Mater.,* **11**(1), 29-43. https://doi.org/10.1007/s40069-016-0179-y.

Pantelides, C.P., Garfield, T.T., Richins, W.D., Larson, T.K. and Blakeley, J.E. (2014), "Reinforced concrete and fiber reinforced concrete panels subjected to blast detonations and post-blast static tests", *Eng. Struct.,* **76**, 24-33. https://doi.org/10.1016/j.engstruct.2014.06.040.

Remennikov, A., Ngo, T., Mohotti, D., Uy, B. and Netherton, M. (2017), "Experimental investigation and simplified modeling of response of steel plates subjected to close-in blast loading from spherical liquid explosive charges", *Int. J. Impact Eng.,* **101**, 78-89. https://doi.org/10.1016/j.ijimpeng.2016.11.013.

Schwer, L. (2010), *An Introduction to the Winfrith Concrete Model*. Schwer Engineering & Consulting Services, California, USA. Streamlit Inc., n. d. https://streamlit.io/.

Thai, D.K. and Kim, S.E. (2018), "Numerical investigation of the damage of RC members subjected to blast loading", *Eng. Fail. Anal.,* **92**, 350-367. https://doi.org/10.1016/j.engfailanal.2018.06.001.

Thai, D.K., Nguyen, D.L. and Nguyen, D.D. (2020), "A calibration of the material model for FRC", *Construct. Build. Mater.,* **254**. https://doi.org/10.1016/j.conbuildmat.2020.119293.

Thai, D.K., Nguyen, D.L., Pham, T.H. and Doan, Q.H. (2021), "Prediction of residual strength of FRC columns under blast loading using the FEM method and regression approach", *Construct. Build. Mater.,* **276**, 122253. https://doi.org/10.1016/j.conbuildmat.2021.122253.

Thai, D.K., Pham, T.H. and Nguyen, D.L. (2019), "Damage assessment of reinforced concrete columns retrofitted by steel jacket under blast loading", *Struct. Design Tall. Spec. Build.* **29**(1), 1-15. https://doi.org/10.1002/tal.1676.

Thai, D.K., Tu, T.M., Bui, T.Q. and Bui, T.T. (2019), "Gradient tree boosting machine learning on predicting the failure modes of the RC panels under impact loads", *Eng. Comput.,* **37**(1), 597-608. https://doi.org/10.1007/s00366-019-00842-w.

Yao, W., Sun, W., Shi, Z., Chen, B., Chen, L. and Feng, J. (2020). "Blast-Resistant Performance of Hybrid Fiber-Reinforced Concrete (HFRC) Panels Subjected to Contact Detonation", *Appl. Sci.,* **10**(1), 1-17. https://doi.org/10.3390/app10010241.

Zhang, H. and Chen, Z. (2021), "Comparison and prediction of seismic performance for shear walls composed with fiber

reinforced concrete", *Adv. Concrete Construct.,* **11**(2), 111-126.
http://dx.doi.org/10.12989/acc.2021.11.2.

*CC*